

Temperature dependence of the optical phonon reflection band in GaP

Cite as: J. Vac. Sci. Technol. B 39, 052201 (2021); doi: 10.1116/6.0001118

Submitted: 5 May 2021 · Accepted: 8 July 2021 ·

Published Online: 26 July 2021



Nuwanjula S. Samarasingha^{a)}  and Stefan Zollner^{b)} 

AFFILIATIONS

Department of Physics, New Mexico State University, P.O. Box 30001, Las Cruces, New Mexico 88003

^{a)}Author to whom correspondence should be addressed: sandu87@nmsu.edu

^{b)}Electronic mail: zollner@nmsu.edu

ABSTRACT

We explore the effect of temperatures between 80 and 720 K on the energy and linewidth of zone-center transverse (TO) and longitudinal (LO) optical phonons in bulk gallium phosphide (GaP) using Fourier transform infrared ellipsometry from 0.03 to 0.60 eV. We extract the optical phonon parameters of GaP by fitting the ellipsometric angles with the Lowndes–Gervais model, which applies two different broadening parameters to the TO and LO phonons. In GaP, the two-phonon density of states is larger for the decay of TO phonons than for LO phonons. Therefore, we observed a larger TO phonon broadening (compared to the LO phonon) and an asymmetric reststrahlen line shape. This would lead to a negative imaginary part of the dielectric function just above the LO phonon energy but the addition of two-phonon absorption avoids this. We find a temperature-dependent redshift and broadening of TO and LO phonons with increasing temperature due to thermal expansion and anharmonic phonon-phonon scattering, involving three and four phonon decay processes. We also investigate the temperature dependence of the high-frequency dielectric constant. Its variation is explained by thermal expansion and the temperature dependence of the Penn gap.

Published under an exclusive license by the AVS. <https://doi.org/10.1116/6.0001118>

I. INTRODUCTION

Most insulators and non-conducting polar semiconductors exhibit bands of high reflectance in the far- or mid-infrared spectral range. These so-called *reststrahlen* bands extend from the energy of transverse optical (TO) phonons to that of the corresponding longitudinal optical (LO) phonons. They have been studied extensively for many materials.^{1–8}

One open question regarding these reststrahlen bands is the relative magnitude of the broadening parameters of the TO and LO phonons. Lowndes¹ and Schubert² explain that the sum of the broadenings γ_{TO} of the TO phonons must be smaller than the sum of the broadenings γ_{LO} of the LO phonons. Berreman and Unterwald³ call this the “passivity” condition, ensuring that the imaginary part of the dielectric function $\epsilon(\omega)$ does not become negative. This condition is satisfied for alkali halides.¹

It is often violated for other materials, however, as shown by Lockwood *et al.*⁴ for six different zinc blende semiconductors using infrared reflectance measurements at oblique incidence combined with a derivative analysis technique, where $\gamma_{\text{TO}} > \gamma_{\text{LO}}$ is found for AlAs, GaP, InP, InAs, and InSb. For highly ordered

materials, such as zinc blende semiconductors, these broadenings are lifetime broadenings, related to the decay of optical phonons into acoustic ones.⁹ For GaP, the decay of TO phonons into two acoustic phonons is very fast because a maximum of the two-phonon density of states (DOS) occurs at the TO energy.^{10,11} By contrast, the two-phonon DOS is lower at the LO energy and, therefore, $\gamma_{\text{TO}} > \gamma_{\text{LO}}$ for GaP. As we will show below, the resulting negative ϵ_2 above the LO energy is compensated by two-phonon absorption.

To further investigate the broadenings of the reststrahlen bands in semiconductors, we measured the temperature dependence of the dielectric function of GaP in the mid-infrared spectral region from 80 to 720 K. We selected GaP for our study because its reststrahlen band is at rather high energies (due to the low mass of the P atom) and Fourier-transform infrared (FTIR) ellipsometry measurements can, therefore, be performed using commercial instrumentation. Furthermore, the reststrahlen band is not distorted by two-phonon absorption between the TO and LO energies.¹² We find a redshift and broadening of the TO and LO phonons due to thermal expansion and anharmonic phonon decay.

Gallium phosphide (GaP) is an isotropic indirect III/V compound semiconductor with a bandgap E_g of approximately 2.25 eV at room temperature.^{13,14} It crystallizes in the zinc blende structure^{13,15} with the cubic space group T_d^2 . GaP has two atoms per primitive cell, resulting in three-fold degenerate acoustic and optical phonon modes at Γ . The polar Fröhlich interaction splits the optical modes into a TO doublet and an LO singlet,^{16,17} which are both Raman- and infrared-active. Throughout this paper, we refer to these infrared- and Raman-active phonons as “optical phonons.” This thermally stable indirect wide bandgap material is an excellent semiconductor for optoelectronic and photonic applications, especially in light-emitting diodes (LEDs),¹⁸ detectors, solar cells, and high-temperature transistors.¹⁴ It is, therefore, important to study the optical properties of this semiconductor, including the effects of cryogenic and elevated temperatures.

Since the TO and LO phonons are both infrared- and Raman-active, they can be studied with infrared reflection, transmission, or ellipsometry as well as Raman scattering, as demonstrated by Barker.⁷ In reflection measurements, one observes a band of high reflection from the TO energy to just above the LO energy. The precise location of the upper end of the reststrahlen band depends on the angle of incidence.² In infrared transmission experiments (of very thin GaP layers), one observes an absorption band at the TO energy defined by $\varepsilon_2(\omega)$. At the LO energy, where $\varepsilon_1(\omega) = 0$, there is a similar peak in the loss function $-\text{Im}[1/\varepsilon(\omega)]$ but light does not couple with LO phonons to lowest order. In infrared ellipsometry measurements, the ellipsometric angle ψ forms a reststrahlen band similar to that found in reflectance measurements, while the ellipsometric angle Δ usually transitions from 180° at low energies (due to the high value of the static dielectric constant) to 0° at high energies (due to the low value of the high-frequency dielectric constant) but this statement is not true for small or very large angles of incidence. For measurements on bulk substrates, the ellipsometric angles can directly be converted into the complex dielectric function and the loss function. No fitting is required.

TO and LO phonons also cause Raman peaks in inelastic light scattering spectra. As explained by Barker and Loudon,^{7,19} $\varepsilon_2(\omega)$ determines the Raman line shape of the TO phonon, while $-\text{Im}[1/\varepsilon(\omega)]$ governs the LO Raman line, see Fig. 2 in Barker.⁷ Therefore, it should be possible to directly compare the Raman energies and linewidths with the energies and linewidths of the peaks in $\varepsilon_2(\omega)$ and $-\text{Im}[1/\varepsilon(\omega)]$ determined with infrared ellipsometry. This is a fundamental premise for the work described in this article.

The vibrational properties of bulk GaP have already been studied theoretically and experimentally by several authors. Using FTIR reflectance, Lockwood *et al.*⁴ investigated TO and LO phonons in several III-V semiconductor materials, including bulk GaP, in the reststrahlen region at room temperature. Bairamov *et al.*^{20,21} measured the effect of temperature on the optical phonon frequency and linewidth with Raman scattering and explained their results with the anharmonic decay of optical phonons into two or three acoustic phonons. They found a redshift and increasing broadening with increasing temperature from 4.2 to 550 K and also an increasing asymmetry of the TO phonon at high temperatures. Debernardi^{9,10} calculated the temperature and pressure dependence of the Raman linewidths and energies of the TO and LO phonons from 0 to 325 K. From the observation of first order Raman spectra, Mooradian and

Wright²² found almost no phonon frequency shift between room temperature and helium temperature. The spectral range of most of these works is around the reststrahlen band ($250\text{--}550\text{ cm}^{-1}$) of bulk GaP. However, several other theoretical and experimental studies of optical phonons in bulk GaP exist,^{23–27} including inelastic neutron scattering data and shell model calculations.¹⁵ Some of them identified not only the long-wavelength optical phonons at the Γ point of the Brillouin zone but also zone edge phonons.^{7,28,29}

II. EXPERIMENTAL METHODS AND MODELS

A bulk unintentionally doped single side polished GaP wafer grown by the liquid encapsulated Czochralski method with 0.5 mm thickness, (111) surface orientation, and a (110) flat was obtained commercially (MTI Corporation, Richmond, CA). The sample had n-type conductivity with an electron concentration on the order of $n = 5 \times 10^{16}\text{ cm}^{-3}$ and a resistivity of about $0.3\ \Omega\text{cm}$. By comparison, the electron concentrations of GaP used for similar studies in the literature range from 10^{16} to 10^{17} cm^{-3} . The electron density may influence the observed phonon line broadenings.

The ellipsometric angles Ψ and Δ of the as-received GaP wafer were acquired (without cleaning) on a J. A. Woollam FTIR Mark II ellipsometer from 0.03 to 0.60 eV (mid and near infrared spectral regions) with 1 cm^{-1} resolution from 80 to 720 K with 25 K step size (30 measurements) inside an ultrahigh vacuum cryostat (Janis ST-400) with diamond windows (Diamond Materials GmbH, Freiburg, Germany) at 70° angle of incidence.² At each temperature, measurements were performed with 15 positions per revolution of the rotating compensator. To increase the signal-to-noise ratio, we averaged 50 interferometer mirror scans at each compensator position. Systematic errors were reduced with $P = \pm 45^\circ$ polarizer angles and also zone averaging the analyzer ($A = 0^\circ, 90^\circ$). WVASE32 (J. A. Woollam Co., Lincoln, NE) and IGOR Pro (WaveMetrics, Lake Oswego, OR) scientific data analysis software were used to analyze our data.

We first measured Ψ and Δ in air at three different incidence angles of 60° , 65° , and 70° to calibrate the cryostat windows.³⁰ The GaP sample was then attached to a copper cold finger using metal clamps. The temperature was measured with two type-E (nickel-chromium/constantan) thermocouples. One located near the cryogen reservoir was used to control the temperature with a Lakeshore temperature controller. The second thermocouple was directly attached to the surface of the GaP sample and measured the temperature of the sample surface. The difference between both thermocouple readings was up to 60 K at the highest temperatures.

The cryostat was then sealed and pumped to a pressure below 10^{-5} Torr. In order to reduce the surface contamination, the sample was heated to 700 K for several hours with a $50\ \Omega$ resistor installed in the cryostat. This anneal may change the surface reconstruction but no serious degradation of the sample is expected.³¹ The cryostat was then allowed to cool down to room temperature while continuing to pump. Once a sufficiently low base pressure of $10^{-9}\text{--}10^{-8}$ Torr was reached, we started to cool the system down to 80 K using liquid nitrogen. Measurements were then taken from low to high temperatures in steps of about 25 K. Typical results at 300 K in air are shown in Fig. 1.

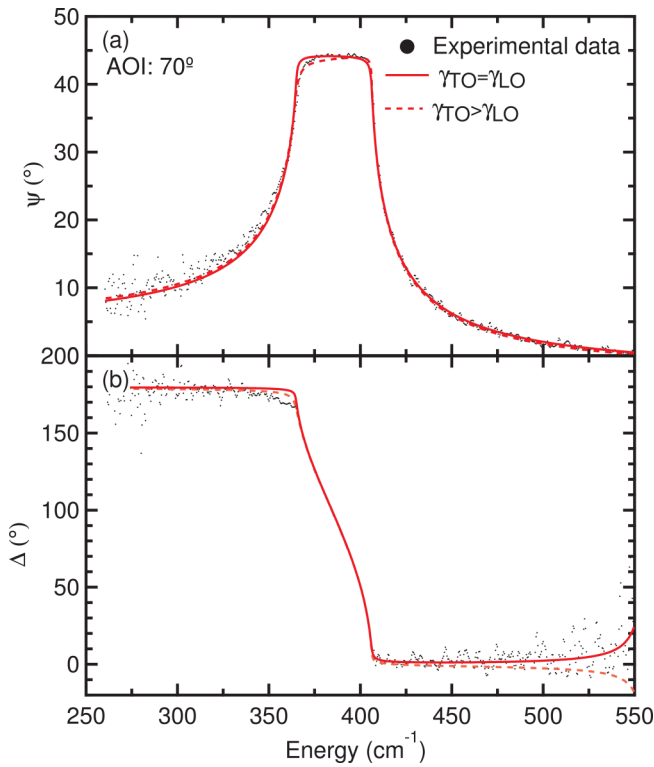


FIG. 1. Ellipsometric angles (a) ψ and (b) Δ at 300 K in air at 70° angle of incidence (AOI) for bulk GaP with a surface layer. The symbols show experimental data. Solid and dashed lines show the result of a fit using Eq. (2).

The static and high-frequency dielectric constants ϵ_s and ϵ_∞ and the optical phonon parameters (amplitude A , TO and LO phonon energies ω_{TO} and ω_{LO} , and corresponding broadenings γ_{TO} and γ_{LO}) were obtained by fitting the ellipsometric angles of GaP at each temperature either with a single Lorentzian,

$$\epsilon(\omega) = \epsilon_\infty + \frac{A\omega_{TO}^2}{\omega_{TO}^2 - \omega^2 - i\gamma_{TO}\omega}, \quad (1)$$

or with the Lowndes–Gervais model,^{1,5}

$$\epsilon(\omega) = \epsilon_\infty \frac{\omega_{LO}^2 - \omega^2 - i\gamma_{LO}\omega}{\omega_{TO}^2 - \omega^2 - i\gamma_{TO}\omega}. \quad (2)$$

Details of this approach are given in Ref. 8 and in the supplementary material.⁶¹ A thin surface overlayer with variable thickness (about 35 Å), described as a 50/50 mixture of GaP and voids within the Bruggeman effective medium approximation, was also included in the model.^{32,33}

Once the surface layer thickness and phonon parameters have been determined from this model for each temperature, it is also possible to fix the surface layer thickness and fit the ellipsometric angles with the optical constants at each photon energy as

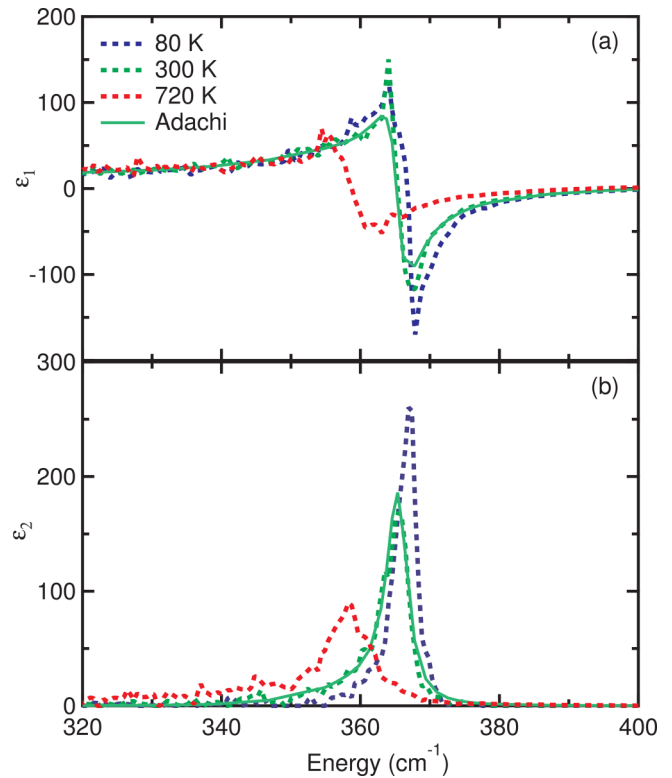


FIG. 2. (a) Real and (b) imaginary parts of the complex dielectric function of bulk GaP at three different temperatures vs photon energy (dashed), determined from a “point-by-point” fit, in comparison with room temperature results as described in Ref. 34 (solid).

parameters. This so-called “point-by-point fit” leads to results in Fig. 2. It can be seen clearly that the extrema of ϵ_1 and ϵ_2 show a redshift, increasing broadening, and decreasing amplitude with increasing temperature. Tabulated optical constants³⁴ are shown for comparison.

III. RESULTS AND DISCUSSION

A. Optical phonon parameters at 300 K

We used four different models to extract the phonon parameters from the experimental data with results shown in Table I for room temperature. Models (1) and (4) fit the ellipsometric angles ψ and Δ with consideration of the experimental errors³³ to Eqs. (1) and (2), respectively. This is the most common data analysis method for ellipsometry data. Models (2) and (3) fit $\langle \epsilon_2(\omega) \rangle$ and $-\text{Im}[1/\langle \epsilon(\omega) \rangle]$ with Lorentzians to determine the TO and LO phonon parameters, respectively. These results should be comparable with the Raman results of Bairamov *et al.*²⁰ A detailed comparison of results from the four models follows below.

The Lorentz model allowed us to find ϵ_∞ , A , ω_{TO} , and γ_{TO} at room temperature either by fitting the ellipsometric angles with the experimental errors (model 1) or only the imaginary part (ϵ_2) of

TABLE I. Phonon parameters at 300 K determined with different models: (1) TO phonon parameters obtained from the Lorentz model by fitting the ellipsometric angles with the experimental errors. ω_{LO} was calculated from Eq. (S5) (Ref. 61). (2) Same, but from fitting only $\langle \epsilon_2 \rangle$. (3) LO phonon parameters from a Lorentzian fit to the pseudo-loss function. (4) Results from the Lowndes–Gervais model, Eq. (2). Data from the literature are also shown. Probable errors are listed in parentheses.

Model	ϵ_∞	A	ω_{TO} (cm^{-1})	γ_{TO} (cm^{-1})	ω_{LO} (cm^{-1})	γ_{LO} (cm^{-1})
(1)	9.02(1)	1.950(2)	364.81(3)	1.61(3)	402.33(6)	NA
(2)	NA	1.97(3)	365.24(3)	3.86(8)	NA	NA
(3)	NA	0.0211(1)	NA	NA	402.3(2)	0.88(1)
(4)	9.02(1)	NA	364.81(3)	2.91(4)	402.33(2)	0.90(3)
Reference 4	9.24(2)		366.3(3)	2.6(6)	402.50(5)	1.2(1)
Reference 7	9.09	1.92	365.3	1.1	402.2	
Reference 20 ^{a,b}			364.5	3.5	402.5	2
Reference 22 ^a			367.3		403.0	
Reference 35	9.091		363.4			
Reference 36 ^c				>4		0.76

^aRaman scattering.

^b $n = 9 \times 10^{16} \text{ cm}^{-3}$ (increased LO broadening).

^cCoherent anti-Stokes Raman scattering.

the pseudo-dielectric function (model 2). Both models yield similar results, see Table I, but γ_{TO} is smaller when fitting the ellipsometric angles (model 1). The Lorentzian broadening affects both the lower and upper corner of the reststrahlen band. If $\gamma_{TO} > \gamma_{LO}$, model (1) will find an intermediate Lorentzian broadening close to the average of γ_{TO} and γ_{LO} . On the other hand, if we only fit $\langle \epsilon_2 \rangle$ in model (2), we find the larger broadening γ_{TO} of the TO phonon. This explains why models (1) and (2) report different values for γ_{TO} , see Table I.

These models (1 and 2) assume equal broadenings for the TO and LO phonons. Results from the Lorentz model (1) are shown by the solid lines in Fig. 1. This model (1) fits the ellipsometric angles near the LO energy well but not near the TO energy. The Lorentzian line shape is symmetric, while the ellipsometric angle ψ is more rounded at the TO energy (indicating a larger broadening) than at the LO energy.

Following Fig. 2 in Barker,⁷ we also determined the energy and broadening of the LO phonon by fitting the pseudo-loss function (S6) with a Lorentzian, see Fig. S1 in the supplementary material.⁶¹ Results are shown in model (3) of Table I. We find that γ_{TO} is two to four times larger than γ_{LO} . This motivates the use of the Lowndes–Gervais model (4), see Eq. (2), to fit the ellipsometric angles because it treats γ_{TO} and γ_{LO} as two independent parameters. These results are shown by the dashed line in Fig. 1 and in model (4) of Table I.

Our value of $\epsilon_\infty = 9.02 \pm 0.01$ is only about 0.8% smaller than $\epsilon_\infty = 9.091$ determined by Parsons and Coleman³⁵ and Borghesi and Guizzetti.³⁷ A better accuracy should not be expected for spectroscopic ellipsometry and can only be obtained with minimum-deviation prism measurements.³⁸ Using the LST relation (S3) (Ref. 61), we find a static dielectric constant $\epsilon_s = 10.97$, also slightly (1.6%) smaller than $\epsilon_\infty = 11.147$ found with far-infrared measurements.^{35,37} The temperature dependence of these dielectric constants will be discussed later within the context of Fig. 6. Our value for $\omega_{LO} = 402.33 \pm 0.06 \text{ cm}^{-1}$ agrees to within 0.1 cm^{-1}

with Lockwood *et al.*,⁴ Parsons and Coleman,³⁵ and Borghesi and Guizzetti³⁷ but differences in the literature for ω_{TO} are several wave numbers. This is unexpected since the upper end of the reststrahlen band near ω_{LO} depends on the angle of incidence and on the free electron concentration (see the supplementary material⁶¹), while the lower end of this band should unambiguously yield ω_{TO} .

It can be seen in Fig. 1 (dashed lines) that the reststrahlen band for bulk GaP is asymmetric, a clear indication that the TO and LO phonon broadenings are different. We can also see an asymmetry of ϵ_2 in Fig. 2. We obtained a better fit (dashed line in Fig. 1) to our data with larger TO broadening ($\gamma_{TO} > \gamma_{LO}$). The mean squared error³³ (difference between model and measured ellipsometric angles, weighted with the experimental errors) is about 10% smaller with the Lowndes–Gervais model than when fitting with a single Lorentzian. The same observation ($\gamma_{TO} > \gamma_{LO}$) was made by others⁴ not only for GaP but also for four other zinc blende semiconductors. Only GaAs is an exception and fulfills the Lorentzian condition $\gamma_{TO} \approx \gamma_{LO}$. Raman scattering measurements of GaP at room temperature⁷ also find $\gamma_{TO} > \gamma_{LO}$. The TO and LO Raman line shapes closely follow the peaks of the imaginary part of the dielectric function and the loss function, respectively.⁷

We interpret the GaP phonon broadenings as pure lifetime broadenings similar to the radiative broadenings discussed by Loudon.³⁹ (See the supplementary material⁶¹ for a discussion of other potential contributions to the broadenings.) The TO phonon energy at the Γ -point in the Brillouin zone is at a maximum of the two-phonon density of states. It is almost exactly the same as the sum of the longitudinal and transverse acoustic (LA+TA) phonon energies at the X -point. Therefore, the TO phonon can decay very efficiently into two acoustic phonons, while the same is not true for the LO phonon.¹¹ The complex self-energy $D(\omega_{TO})$ has a large imaginary part. This explains $\gamma_{TO} > \gamma_{LO}$.

The phonon dephasing time τ is related to its broadening by^{36,40} $\gamma = 2\hbar/\tau$, where $\hbar = 0.658 \text{ meVps}$ is the reduced Planck's constant. The LO phonon lifetime should, therefore, be larger than

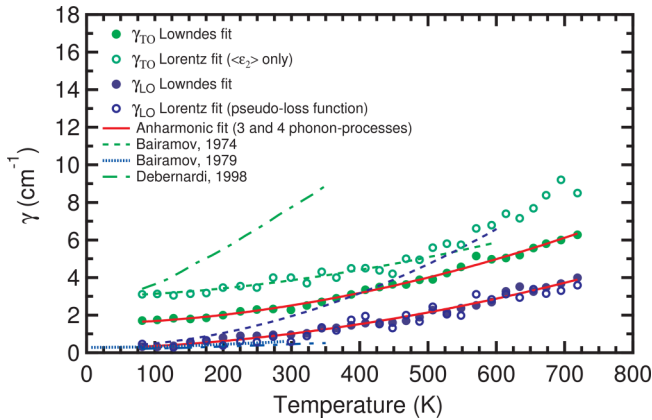


FIG. 4. Temperature dependence of the TO and LO phonon broadenings (symbols). Solid lines show the best fit to our data using Eq. (3) with parameters in Table II. Raman linewidths from Refs. 20 and 21 are shown by dashed and dotted lines, respectively. The dashed-dotted lines show results from density-functional perturbation theory.^{9,10}

results obtained by fitting the ellipsometric angles with a Lowndes model (2). Open circles show results obtained by fitting $\langle \epsilon_2 \rangle$ and the pseudo-loss function with a Lorentzian. Both methods yield the same values for the LO phonon broadenings but the TO broadenings found from fitting $\langle \epsilon_2 \rangle$ are significantly larger than when fitting the ellipsometric angles. This discrepancy is discussed in detail in the supplementary material.⁶¹

Our LO broadenings closely follow the 1979 results by Bairamov *et al.*,²¹ Kuhl and Bron,³⁶ and Vallée⁴⁹ obtained from Raman linewidths or coherent anti-Stokes Raman scattering decay times of high-purity GaP samples (dotted). Earlier Raman work²⁰ used a GaP sample with a higher electron concentration of $9 \times 10^{16} \text{ cm}^{-3}$, where the LO broadening is increased due to plasmon-phonon coupling (dashed). The Raman broadenings of the TO phonon²⁰ (dashed) are not affected by doping. They follow our results for fitting $\langle \epsilon_2 \rangle$ with a Lorentzian (open symbols) since the Raman line shape closely follows ϵ_2 , see Ref. 7.

Debernardi^{9,10} calculated the temperature and pressure dependence of the Raman linewidths and energies of the TO and LO phonons from 0 to 325 K, as shown by the dashed-dotted lines. However, his calculated linewidths for the TO phonon agree with Bairamov *et al.*²⁰ only at low temperatures and are much larger than the experimental results at higher temperatures. In the case of the LO phonon linewidths, the agreement with experiment^{21,36,49} is much better.

Empirically, the broadenings due to anharmonic decay can be fitted with the following expression:^{20,47,50}

$$\gamma(T) = \gamma_0 + A \left[1 + \frac{2}{e^x - 1} \right] + B \left[1 + \frac{3}{e^y - 1} + \frac{3}{(e^y - 1)^2} \right], \quad (3)$$

where A and B are three- and four-phonon coupling constants,

TABLE II. Anharmonic decay parameters for Eq. (3) for the temperature dependence of TO and LO phonon broadenings. Errors are shown in parentheses. Energies marked (f) were fixed during the fit, compare Table III.

This work	TO	LO
$A \text{ (cm}^{-1}\text{)}$	0.2(1)	0.2(f)
$B \text{ (cm}^{-1}\text{)}$	0.08(1)	0.069(2)
$\gamma_0 \text{ (cm}^{-1}\text{)}$	1.4(1)	0.03(4)
$\omega_0 \text{ (cm}^{-1}\text{)}$	367.3(f)	406.6(f)
Reference 20	TO	LO
$A \text{ (cm}^{-1}\text{)}$	0.20	0.16
$B \text{ (cm}^{-1}\text{)}$	0.06	0.20
$\gamma_0 \text{ (cm}^{-1}\text{)}$	2.8	0
$\omega_0 \text{ (cm}^{-1}\text{)}$	366	404

respectively. The reduced phonon energies x and y are

$$x = \frac{\hbar\omega_0}{2k_B T} \quad \text{and} \quad y = \frac{\hbar\omega_0}{3k_B T}, \quad (4)$$

where ω_0 is the unrenormalized phonon frequency and k_B is the Boltzmann constant. The parameter γ_0 describes temperature-independent mechanisms such as inhomogeneous broadening due to defects or the instrumental resolution. Table II lists the best-fit parameters of Eq. (3) for TO and LO phonons. The broadenings calculated with these parameters (shown by the solid lines in Fig. 4) agree very well with the experimental results. Our anharmonic parameters A and B agree well with those in Ref. 20 for the TO phonon (except for a constant shift related to a different value for γ_0 due to a different fitting method), but our parameter B is much smaller for the LO phonon since our sample had a lower doping concentration than in Ref. 20.

2. Temperature dependence of phonon energies

The temperature dependence of the optical phonon energies due to thermal expansion (TE) is given by^{48,51,52}

$$\omega_{\text{TE}}(T) = \omega_0 \exp \left[-3\gamma \int_0^T \alpha_l(\theta) d\theta \right], \quad (5)$$

where ω_0 is the phonon energy at 0 K, γ the Grüneisen parameter for the phonon mode, and α_l the linear thermal expansion coefficient. Since thermal expansion is small, it suffices²⁰ to keep only the linear term in the exponential in Eq. (5).

The thermal expansivity can be described using a Debye model for the phonons⁵³

$$\alpha_l(T) = \alpha_{l\infty} D \left(\frac{\Theta_D}{T} \right), \quad (6)$$

where $\Theta_D = 440 \text{ K}$ is the Debye temperature, $\alpha_{l\infty} = 5.8 \times 10^{-6} \text{ K}^{-1}$ the thermal expansion coefficient in the high temperature limit,

and^{20,53}

$$D(\eta) = \frac{3}{\eta^3} \int_0^\eta \frac{e^{\xi} \xi^4}{(e^{\xi} - 1)^2} d\xi. \quad (7)$$

Instead, we can also use tabulated values^{10,54,55} for the thermal expansion coefficient and perform the integration in Eq. (5) numerically.

The dependence of TO and LO phonon energies on temperature determined from a Lowndes fit to the ellipsometric angles is shown in Fig. 5 (symbols). Both show a redshift (decrease) with increasing temperature. The contribution of thermal expansion to these redshifts (dashed) is not sufficient to explain the experimental data. Therefore, Bairamov *et al.*²⁰ also included three- and four-phonon anharmonic decay processes.

The anharmonic contribution to the redshift can be described as⁴⁷

$$\omega(T) = \omega_0 - C \left[1 + \frac{2}{e^x - 1} \right] - D \left[1 + \frac{3}{e^y - 1} + \frac{3}{(e^y - 1)^2} \right], \quad (8)$$

where C and D are the anharmonic coupling strengths. The second and third terms in Eq. (8) relate to three- and four-phonon decay processes, respectively. Setting $D=0$ (i.e., ignoring four-phonon processes) does not achieve a good fit.

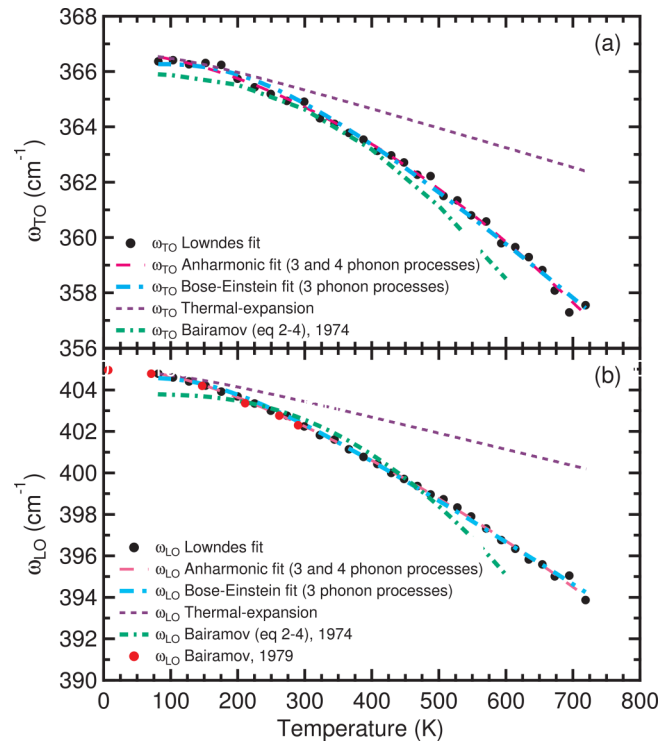


FIG. 5. Temperature dependence of the (a) transverse (ω_{TO}) and (b) longitudinal (ω_{LO}) optical phonon energies of GaP (symbols). The dashed line shows the contribution of thermal expansion. Fits using Eqs. (8) and (9) with parameters in Table III are shown by dashed-dotted lines.

TABLE III. Anharmonic decay parameters for the temperature dependence of TO and LO phonon energies. Errors are shown in parentheses.

Anharmonic decay parameters	TO	LO
This work, Eq. (8), ignoring thermal expansion		
ω_0 (cm^{-1})	367.3(2)	406.6(1)
C (cm^{-1})	0.5(1)	1.6(1)
D (cm^{-1})	0.14(1)	0.11(1)
Reference 20, Eq. (8), Raman, thermal expansion subtracted		
ω_0 (cm^{-1})	364.5	401.4
C (cm^{-1})	-1.76	-2.98
D (cm^{-1})	0.30	0.51
This work, Eq. (9), ignoring thermal expansion		
ω_0 (cm^{-1})	374.6(8)	410.5(4)
C (cm^{-1})	8.3(9)	5.9(4)
ω_{eff} (cm^{-1})	530(30)	380(20)

In principle, one should subtract the redshift due to thermal expansion from the observed redshift and then fit the parameters C and D . This was done by Bairamov *et al.*,²⁰ which resulted in the parameters shown in Table III. In practice, however, one often ignores the thermal expansion contribution⁴⁷ and directly fits the experimental data with Eq. (8). These parameters are also shown in Table III. The two methods result not only in different sets of coupling constants C and D but also in differences for the unrenormalized phonon energies ω_0 .

This redshift can also be fitted empirically with a Bose-Einstein expression⁵⁶

$$\omega(T) = \omega_0 - C \left[1 + \frac{2}{e^{\frac{\theta_B}{T}} - 1} \right] \quad (9)$$

as an anharmonic three-phonon decay with an adjustable effective phonon energy $\omega_{\text{eff}} = k_B \theta_B$, where θ_B is an effective phonon temperature related to the Debye temperature of GaP (440 K). These results are also shown in Table III.

3. Temperature dependence of high-frequency and static dielectric constants

The high-frequency dielectric constant ϵ_∞ for bulk GaP was also obtained from fitting the ellipsometric angles at each temperature with Lowndes model (2). It increases with temperature, as shown in Fig. 6. ϵ_∞ can be expressed as⁵⁷

$$\epsilon_\infty = 1 + \left(\frac{E_u}{E_{\text{Penn}}} \right)^2, \quad (10)$$

where the unscreened plasma frequency of the valence electrons is given by

$$E_u^2 = \hbar^2 \omega_u^2 = \frac{\hbar^2 N e^2}{m_0 \epsilon_0} = (16.5 \text{ eV})^2, \quad (11)$$

where N is the density of valence electrons per unit volume (eight electrons per formula unit), e the charge of the electron, m_0 the

free electron mass, and ϵ_0 the vacuum permittivity. The resulting Penn gap $E_{\text{Penn}} = 5.83$ eV, calculated from ϵ_∞ at 300 K, is the average separation between the valence and conduction bands across the Brillouin zone, usually located near the E_2 gap (5.28 eV for GaP, see Refs. 57 and 58). We assume that E_2 and E_{Penn} have the same temperature dependence.

Taking the derivative of Eq. (10) with respect to temperature yields^{59,60}

$$\frac{d\epsilon_\infty}{dT} = -3\alpha_l(\epsilon_\infty - 1) - 2(\epsilon_\infty - 1)\frac{d\ln E_2}{dT}. \quad (12)$$

The first term considers the decrease of the electron density due to thermal expansion, which results in a decrease of ϵ_∞ . The second term describes the increase of ϵ_∞ due to the decrease of the Penn gap with increasing temperature. This is the dominant term.

We calculated the temperature dependence of ϵ_∞ at room temperature, resulting in

$$\left. \frac{d\epsilon_\infty}{dT} \right|_{300\text{K}} = (-1.2 + 7.6) \times 10^{-4} \text{ K}^{-1} = 6.4 \times 10^{-4} \text{ K}^{-1}. \quad (13)$$

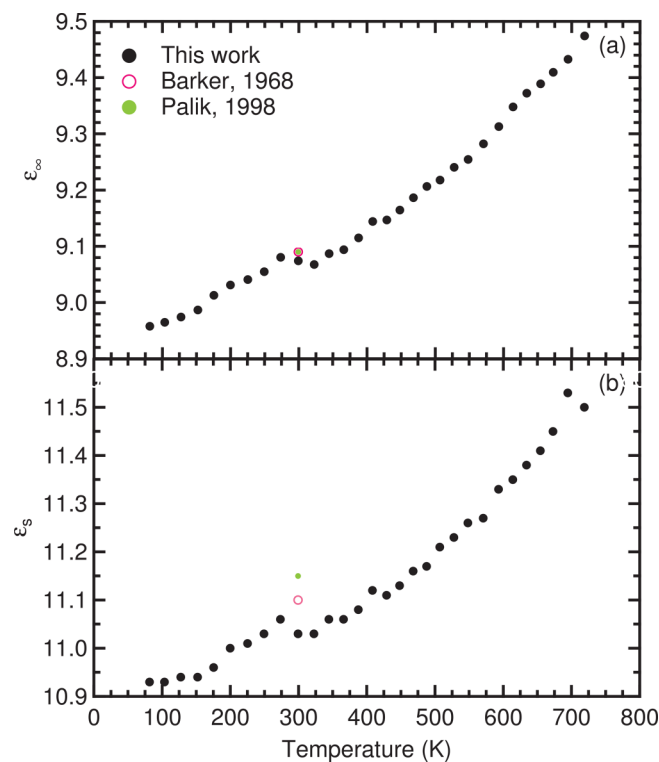


FIG. 6. Temperature dependence of the (a) high-frequency (ϵ_∞) and (b) static (ϵ_s) dielectric constants. ϵ_∞ was found by fitting the experimental data with Eq. (2). ϵ_s was calculated from the Lyddane–Sachs–Teller relation (S3) (Ref. 61). Data from the literature^{7,35,37} are also shown.

This value compares favorably with the experimental variation of ϵ_∞ between 200 and 400 K, which is $4.5 \times 10^{-4} \text{ K}^{-1}$. Therefore, we conclude that model (12) for the temperature dependence of ϵ_∞ is reasonable.

The temperature dependence of ϵ_s was calculated from the Lyddane–Sachs–Teller (LST) relation (S3) (Ref. 61) and is also shown in Fig. 6. Since the ratio of the TO and LO phonon energies does not strongly depend on temperature, the variations of ϵ_s with temperature are very similar to those of ϵ_∞ . We find that ϵ_s changes by about 1% between 0 and 300 K, which is three times larger than the change calculated by Debernardi.¹⁰

IV. SUMMARY

We used FTIR spectroscopic ellipsometry from 0.03 to 0.60 eV to determine the effects of temperature on the properties of long-wavelength optical phonons of GaP at temperatures ranging from 80 to 720 K. With different experimental conditions, we also observed two-phonon absorption. GaP shows an asymmetric reststrahlen line shape because the linewidth of the TO phonon is larger than that of the LO phonon at all temperatures. This violates the Lowndes passivity condition and the imaginary part ϵ_2 of the dielectric function becomes slightly negative just above the LO energy. To achieve a physically meaningful non-negative total dielectric function, we must also add multiphonon absorption to the single phonon absorption. We also observed that the energies of the TO and LO optical phonons show a redshift and increasing broadening with increasing temperature due to thermal expansion and anharmonic phonon-phonon decay. The static and high-frequency dielectric constant increased with increasing temperature because of the thermal expansion of the crystal and the temperature dependence of the Penn gap.

ACKNOWLEDGMENTS

This work was supported by the National Science Foundation (NSF) (No. DMR-1505172) and the US Army (No. W911NF-16-1-0492). We wish to thank Professor David J. Lockwood (National Research Council of Canada) and Professor Sotirios Ves (Aristotle University of Thessaloniki, Greece) for helpful discussions regarding this research topic.

DATA AVAILABILITY

The data that support the findings of this study are available from the corresponding author upon reasonable request.

REFERENCES

- ¹R. P. Lowndes, *Phys. Rev. B* **1**, 2754 (1970).
- ²M. Schubert, *Infrared Ellipsometry on Semiconductor Layer Structures: Phonons, Plasmons, and Polaritons* (Springer, Berlin, 2004).
- ³D. W. Berreman and F. C. Unterwald, *Phys. Rev.* **174**, 791 (1968).
- ⁴D. J. Lockwood, G. Yu, and N. L. Rowell, *Solid State Commun.* **136**, 404 (2005).
- ⁵F. Gervais and B. Piriou, *J. Phys. C Solid State Phys.* **7**, 2374 (1974).
- ⁶A. S. Barker, *Phys. Rev.* **136**, A1290 (1964).
- ⁷A. S. Barker, *Phys. Rev.* **165**, 917 (1968).
- ⁸S. Zollner, P. Paradis, F. Abadizaman, and N. S. Samarasingha, *J. Vac. Sci. Technol. B* **37**, 012904 (2019).

- ⁹A. Debernardi, *Phys. Rev. B* **57**, 12847 (1998).
- ¹⁰A. Debernardi, *Solid State Commun.* **113**, 1 (2000).
- ¹¹S. Ves, I. Loa, K. Syassen, F. Widulle, and M. Cardona, *Phys. Status Solidi B* **223**, 241 (2001).
- ¹²T. I. Willett-Gies, C. M. Nelson, L. S. Abdallah, and S. Zollner, *J. Vac. Sci. Technol. A* **33**, 061202 (2015).
- ¹³C. I. Ribeiro-Silva, A. Picinin, J. P. Rino, M. G. Menezes, and R. B. Capaz, *Comput. Mater. Sci.* **161**, 265 (2019).
- ¹⁴A. R. Aparna, V. Brahmajirao, and T. V. Karthikeyan, *Proc. Mater. Sci.* **6**, 1650 (2014).
- ¹⁵P. H. Borchers, K. Kunc, G. F. Alfrey, and R. L. Hall, *J. Phys. C Solid State Phys.* **12**, 4699 (1979).
- ¹⁶D. Snoke, *Solid State Physics* (Addison-Wesley, San Francisco, 2000).
- ¹⁷J. L. Birman, *Phys. Rev.* **127**, 1093 (1962).
- ¹⁸M. M. Sobolev and V. G. Nikitin, *Tech. Phys. Lett.* **24**, 329 (1998).
- ¹⁹A. S. Barker and R. Loudon, *Rev. Mod. Phys.* **44**, 18 (1972).
- ²⁰B. Kh. Bairamov, Yu. E. Kitaev, V. K. Negoduiko, and Z. M. Khashkhozhev, *Fiz. Tverd. Tela* **16**, 2036 (1974) [*Sov. Phys. Solid State* **16**, 1323 (1975)]. There is a missing exponential in the Debye integral just below Eq. (5) of this paper, compare Ref. 53.
- ²¹B. Kh. Bairamov, D. A. Parshin, V. V. Toporov, and Sh. B. Ubaidullaev, *Pis'ma Zh. Tekh. Fiz.* **5**, 1116 (1979) [*Sov. Tech. Phys. Lett.* **5**, 466 (1979)].
- ²²A. Mooradian and G. B. Wright, *Solid State Commun.* **4**, 431 (1966).
- ²³A. H. Kachare, J. M. Cherlow, T. T. Yang, and W. G. Spitzer, *J. Appl. Phys.* **47**, 161 (1976).
- ²⁴A. K. W. Abdullah, G. A. Gledhill, C. Patel, and T. J. Parker, *Infrared Physics & Technology* **29**, 719 (1989).
- ²⁵M. Hass, *Semiconduct. Semimet.* **3**, 3 (1967).
- ²⁶K. A. Maslin, C. Patel, and T. J. Parker, *Infrared Phys.* **32**, 303 (1991).
- ²⁷M. Giehler and E. Jahne, *Phys. Status Solidi B* **73**, 503 (1976).
- ²⁸B. Pödör, *Phys. Status Solidi B* **120**, 207 (1983).
- ²⁹B. Pödör and V. P. Izvekoy, *Rev. Phys. Appl.* **18**, 737 (1983).
- ³⁰F. Abadizaman, "Optical characterization of Ni using spectroscopic ellipsometry at temperatures from 80 K to 780 K," Ph.D. thesis (New Mexico State University, 2020).
- ³¹Y. Sun, D. C. Law, and R. F. Hicks, *Surf. Sci.* **540**, 12 (2003).
- ³²H. G. Tompkins and J. N. Hilifiker, *Spectroscopic Ellipsometry: Practical Application to Thin-Film Characterization* (Momentum, New York, 2016).
- ³³H. Fujiwara, *Spectroscopic Ellipsometry* (Wiley, Chichester, 2007).
- ³⁴S. Adachi, *Optical Constants of Crystalline and Amorphous Semiconductors* (Springer, New York, 1999).
- ³⁵D. F. Parsons and P. D. Coleman, *Appl. Opt.* **10**, 1683 (1971).
- ³⁶J. Kuhl and W. E. Bron, *Solid State Commun.* **49**, 935 (1984).
- ³⁷A. Borghesi and G. Guizzetti, in *Handbook of Optical Constants of Solids*, edited by E. D. Palik (Academic, New York, 1998).
- ³⁸W. L. Bond, *J. Appl. Phys.* **36**, 1674 (1965).
- ³⁹R. Loudon, *The Quantum Theory of Light* (Oxford, New York, 1984).
- ⁴⁰A. Laubereau and W. Kaiser, *Rev. Mod. Phys.* **50**, 607 (1978).
- ⁴¹D. von der Linde, J. Kuhl, and H. Klingenberg, *Phys. Rev. Lett.* **44**, 1505 (1980).
- ⁴²A. Laubereau, D. von der Linde, and W. Kaiser, *Opt. Commun.* **7**, 173 (1973).
- ⁴³E. S. Koteles and W. R. Datars, *Solid State Commun.* **19**, 221 (1976).
- ⁴⁴M. V. Hobden and J. P. Russell, *Phys. Lett.* **13**, 39 (1964).
- ⁴⁵D. A. Kleinman and W. G. Spitzer, *Phys. Rev.* **118**, 110 (1960).
- ⁴⁶B. Ulrici and E. Jahne, *Phys. Status Solidi B* **86**, 517 (1978).
- ⁴⁷M. Balkanski, R. F. Wallis, and E. Haro, *Phys. Rev. B* **28**, 1928 (1983).
- ⁴⁸J. Menéndez and M. Cardona, *Phys. Rev. B* **29**, 2051 (1984).
- ⁴⁹F. Vallée, *Phys. Rev. B* **49**, 2460 (1994).
- ⁵⁰T. Sakurai and T. Sato, *Phys. Rev. B* **4**, 583 (1971).
- ⁵¹W. J. Borer, S. S. Mitra, and K. V. Namjoshi, *Solid State Commun.* **9**, 1377 (1971).
- ⁵²C. Postmus, J. R. Ferraro, and S. S. Mitra, *Phys. Rev.* **174**, 983 (1968).
- ⁵³R. Roucka, Y.-Y. Fang, J. Kouvetakis, A. V. G. Chizmeshya, and J. Menéndez, *Phys. Rev. B* **81**, 245214 (2010).
- ⁵⁴P. Deus, U. Volland, and H. A. Schneider, *Phys. Status Solidi A* **80**, K29 (1983).
- ⁵⁵O. Madelung, W. von der Osten, and U. Rössler, in *Landolt-Börnstein Numerical Data and Functional Relationships in Science and Technology* (Springer, Berlin, 1987), vol. III/22a; D. Bimberg *et al.*, in *Landolt-Börnstein Numerical Data and Functional Relationships in Science and Technology* (Springer, Berlin, 1982), vol. III/17a.
- ⁵⁶L. Viña, S. Logothetidis, and M. Cardona, *Phys. Rev. B* **30**, 1979 (1984).
- ⁵⁷P. Y. Yu and M. Cardona, *Fundamentals of Semiconductors* (Springer, Berlin, 2010).
- ⁵⁸S. Zollner, M. Garriga, J. Kircher, J. Humlíček, M. Cardona, and G. Neuhold, *Phys. Rev. B* **48**, 7915 (1993).
- ⁵⁹K. Vedam, J. L. Kirk, and B. N. N. Achar, *J. Solid State Chem.* **12**, 213 (1975).
- ⁶⁰C. M. Nelson, M. Spies, L. S. Abdallah, and S. Zollner, *J. Vac. Sci. Technol. A* **30**, 061404 (2012).
- ⁶¹See the supplementary material at <https://www.scitation.org/doi/suppl/10.1116/6.0001118> for additional information regarding analytical models for infrared lattice absorption, frequency-dependent broadening, accurate determination of phonon broadening parameters from ellipsometry data, origins of the phonon broadenings, GaP phonon dispersion, the Born effective charge, and the variation of the apparent GaP surface layer thickness with temperature.

Supplementary Material: Temperature dependence of the optical phonon reflection band in GaP

(*Email:zollner@nmsu.edu)

(*Email:sandu87@nmsu.edu)

(Dated: 24 June 2021)

Nuwanjula S. Samarasingha and Stefan Zollner
Department of Physics, New Mexico State University, P.O. Box 30001, Las Cruces, NM 88003, USA

S1. LORENTZ MODEL FOR A SINGLE PHONON

The static and high-frequency dielectric constants ϵ_s and ϵ_∞ and the optical phonon parameters (amplitude A , TO and LO phonon energies ω_{TO} and ω_{LO} , and corresponding broadenings γ_{TO} and γ_{LO}) were obtained by fitting the ellipsometric angles of GaP at each temperature either with a single Lorentzian or with the Lowndes-Gervais model.^{1,5} The difference between these two models is that the Lowndes-Gervais model assigns two different broadening parameters γ_{TO} and γ_{LO} to the two phonons, while the Lorentz model has only one broadening parameter γ_{TO} .

Following Helmholtz (Ann. Phys. **230**, 582, 1875) or Wooten (*Optical Properties of Solids*, Academic, New York, 1972), the dispersion due to damped vibrations of molecules in a solid under the influence of an electromagnetic wave can be described by a Lorentz oscillator⁷

$$\epsilon(\omega) = \epsilon_\infty + \frac{A\omega_{\text{TO}}^2}{\omega_{\text{TO}}^2 - \omega^2 - i\gamma_{\text{TO}}\omega}. \quad (\text{S1})$$

TO phonons therefore appear as a strong symmetric peak with linewidth γ_{TO} (FWHM) just below ω_{TO} (due to damping) in the imaginary part ϵ_2 of the complex dielectric function.¹² The maximum height of this peak is

$$\epsilon_2(\omega_{\text{TO}}) \approx A \frac{\omega_{\text{TO}}}{\gamma_{\text{TO}}} \quad (\text{S2})$$

for $\gamma_{\text{TO}} \ll \omega_{\text{TO}}$. The peak position ω_{TO} can usually be determined very precisely from the position of the ϵ_2 peak. However, the peak amplitude is influenced by both A and γ_{TO} . In practice, this leads to parameter correlations when fitting data, especially if the peak shape is not precisely Lorentzian (e.g., due to asymmetry).

The minimum and maximum of the real part ϵ_1 of the dielectric function are separated by γ_{TO} . In this region, ϵ_1 shows anomalous dispersion. The LO phonon energy is defined by $\epsilon_1(\omega_{\text{LO}})=0$. It can be found from the Lyddane-Sachs-Teller (LST) relation⁴

$$\epsilon_s = \epsilon_\infty \frac{\omega_{\text{LO}}^2}{\omega_{\text{TO}}^2}. \quad (\text{S3})$$

The real part $\epsilon_1(\omega)$ is negative between ω_{TO} and ω_{LO} . This leads to a region of high reflectivity called reststrahlen band.

Representative graphs of the dielectric function, the complex refractive index, and the reflectivity at normal incidence for a Lorentz oscillator are shown by Wooten (1972). The ellipsometric angles at 70° angle of incidence calculated from the Lorentz model are shown by solid lines in Fig. 1. It is important to note that the Lorentz model shows strong symmetry in the dielectric function, the reflectivity at normal incidence, and in the ellipsometric angles (but not in the complex refractive index or the absorption coefficient). For $\gamma_{\text{TO}}=0$, the reflectance R equals unity and the ellipsometric angle $\psi=45^\circ$ within the reststrahlen band. The corners of R and ψ are very sharp. The rise of ψ or R occurs precisely at the TO frequency, but the drop is pushed beyond the LO frequency at higher angles of incidence.² These corners are rounded symmetrically once γ_{TO} increases and R and ψ are lower than their ideal undamped values. The most precise determination of the broadening parameter γ_{TO} can therefore be made from the ellipsometric angle ψ within the reststrahlen region and its deviation from 45° . This is independent of the value of the amplitude A . Within the reststrahlen band, there is enhanced sensitivity to the low absorption caused by two-phonon processes (J. Humlíček, Thin Solid Films **313-314**, 687, 1998). Setting $\omega=0$ in Eq. (S1), we find the relationship

$$\epsilon_s = \epsilon_\infty + A \quad (\text{S4})$$

between the static ($\omega=0$) and high-frequency ($\omega \rightarrow \infty$) dielectric constants. Combining Eqs. (S3) and (S4), we find

$$\omega_{\text{LO}} = \omega_{\text{TO}} \sqrt{1 + \frac{A}{\epsilon_\infty}}. \quad (\text{S5})$$

As shown in Fig. S1, the pseudo-loss function

$$\text{Im} \left(-\frac{1}{\langle \epsilon \rangle} \right) = -\langle \eta_2 \rangle = \frac{\langle \epsilon_2 \rangle}{\langle \epsilon_1 \rangle^2 + \langle \epsilon_2 \rangle^2} \quad (\text{S6})$$

shows a strong peak at the LO phonon energy (Wooten, 1972). To obtain the amplitude B , energy ω_{LO} , and broadening γ_{LO} of the LO phonon, the experimental data points in the pseudo-loss function (S6) were fitted in IGOR Pro with the imaginary part of a Lorentzian

$$-\langle \eta_2 \rangle = \frac{B\omega_{\text{LO}}^2\gamma_{\text{LO}}\omega}{(\omega_{\text{LO}}^2 - \omega^2)^2 + \gamma_{\text{LO}}^2\omega^2}. \quad (\text{S7})$$

The parameters from this fit are shown in model (3) of Table I. The LO phonon energy of 402.3 cm^{-1} obtained from this pseudo-loss function fit matched perfectly with the calculated value 402.33 cm^{-1} from Eq. (S5).

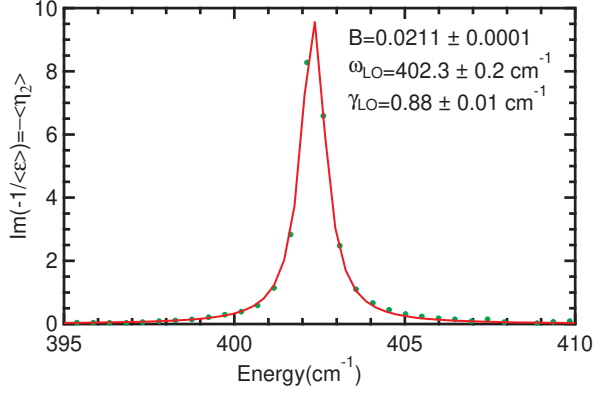


FIG. S1. Pseudo-loss function for GaP in the reststrahlen region at room temperature (in air) fitted with a Lorentzian as in Eq. (S7).

S2. FREQUENCY-DEPENDENT BROADENING

The Lorentz oscillator function (S1) can be solved for the broadening parameter

$$i\gamma\omega = \omega_{\text{TO}}^2 \frac{\epsilon - \epsilon_s}{\epsilon - \epsilon_\infty} - \omega^2. \quad (\text{S8})$$

If ϵ follows a Lorentzian lineshape, then of course this expression (S8) yields a constant γ_{TO} . However, we can also evaluate this expression for other types of lineshapes or from experimental data $\epsilon(\omega) = \epsilon_1 + i\epsilon_2$, if the static and high-frequency dielectric constants ϵ_s and ϵ_∞ are found from extrapolation.

We can break up Eq. (S8) into real and imaginary components²⁶ (see also A. Rastogi, K. F. Pai, T. J. Parker, and R. P. Lowndes, in *Proceedings of the International Conference on Lattice Dynamics, Paris, September 5-9, 1977*, edited by M. Balkanski (Flammarion, Paris, 1978), p. 142)

$$i\gamma\omega = \omega_{\text{TO}}^2 \frac{(\epsilon_1 - \epsilon_s)(\epsilon_1 - \epsilon_\infty) + \epsilon_2^2}{(\epsilon_1 - \epsilon_\infty)^2 + \epsilon_2^2} - \omega^2 + i\omega_{\text{TO}}^2 \frac{(\epsilon_s - \epsilon_\infty)\epsilon_2}{(\epsilon_1 - \epsilon_\infty)^2 + \epsilon_2^2}. \quad (\text{S9})$$

In the anharmonic literature,²⁶ the broadening term

$$i\gamma\omega = 2\omega_{\text{TO}} [\Delta(\omega) + i\Gamma(\omega)] \quad (\text{S10})$$

in the denominator of the Lorentzian lineshape (S1) is typically associated with a complex self-energy $\Delta(\omega) + i\Gamma(\omega)$. In this view, ω_{TO} is the unrenormalized (truly harmonic) resonance frequency of the oscillator. The real part $\Delta(\omega)$ of this self energy has two contributions due to thermal expansion and due to the anharmonic decay of optical phonons into acoustic ones. It usually leads to a redshift of the phonon frequency. The imaginary part $\Gamma(\omega)$ causes a broadening of the phonon resonance, leading to a FWHM of $\gamma_{\text{TO}} \approx 2\Gamma(\omega_{\text{TO}})$.

We first evaluate the broadening γ in Eq. (S9) for a Lowndes lineshape (2), shown by the solid lines in Fig. S2. The Lowndes parameters were taken from fits to our ellipsometric

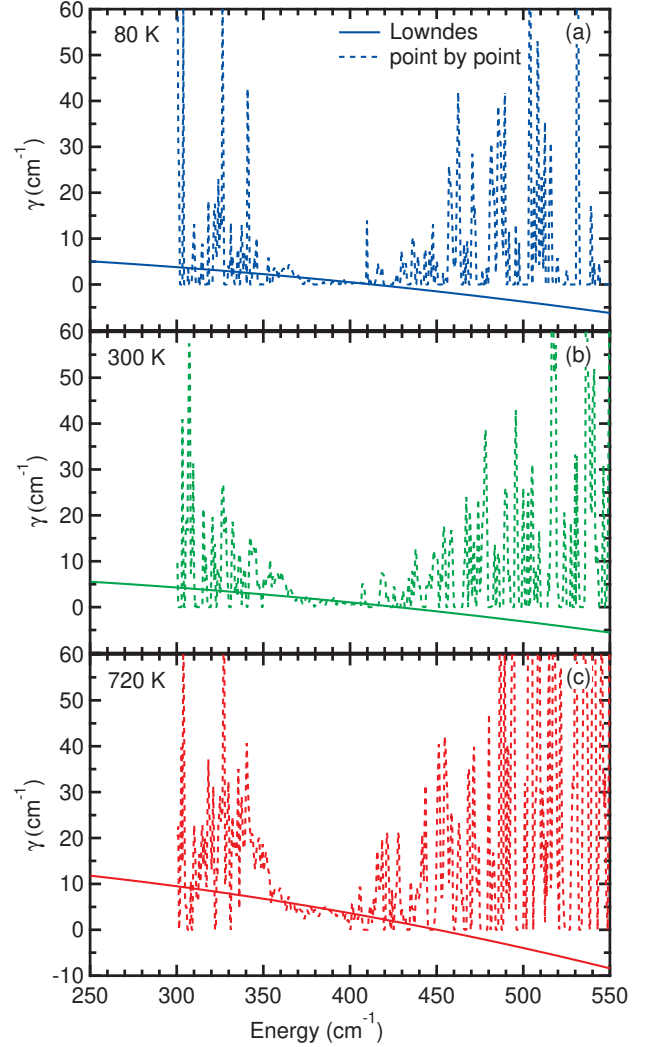


FIG. S2. Frequency-dependent scattering rate of GaP at (a) 80 K, (b) 300 K, and (c) 720 K calculated from the Lowndes lineshape in Eq. (2) (solid) and from our experimental (point-by-point fit) data (dashed) in Fig. 2.

angles at three different temperatures. The broadening parameter decreases steadily with increasing photon energy, since $\gamma_{\text{TO}} > \gamma_{\text{LO}}$, and eventually becomes negative above the LO frequency where $\epsilon_2 < 0$ for our Lowndes parameters. A negative broadening parameter leads to a pole in the dielectric function below the real axis. This is forbidden, because it violates both the causality and the passivity conditions.³ In practice, this is offset by higher-order phonon absorption processes which lead to a positive ϵ_2 as discussed in Sec. III B.

The application of Eq. (S9) to our experimental data is somewhat disappointing, see the dashed lines in Fig. S2. First, we note that γ is always positive, because our ellipsometry fitting software enforces $\epsilon_2 > 0$. The noise is very high above the LO phonon energy, where the reflected light intensity is very low. We have excellent signal-to-noise ratio in the reststrahlen region between ω_{TO} and ω_{LO} , which allows a very accurate

determination of the broadening parameter in this region. The data is also noisy below the TO phonon energy, because this spectral region is at the very edge or even below the specified energy range of our instrument. A better signal-to-noise ratio in FTIR ellipsometry would be needed to study the frequency dependent scattering rate.

The broadening parameter γ increases with increasing temperature and therefore one expects that this technique should yield better results at higher temperatures, where the broadenings are larger. With a bit of imagination, we might indeed locate a peak in the broadening at 720 K below the TO energy, see Fig. S2, where it is expected.⁷ See also Ushioda *et al.*, Phys. Rev. B **8**, 4634 (1973), and Ushioda and McMullen, Solid State Commun. **11**, 299 (1972). Similar results are shown in Ref. 26 for ZnSe and by Ratogi *et al.* (1978) for RbBr and KTaO₃.

S3. ACCURATE DETERMINATION OF THE BROADENING PARAMETER

In Fig. 4, we show the TO and LO broadenings versus temperature fitted to our experimental data using two different methods: (1) We fitted the ellipsometric angles weighted with the experimental errors with the Lowndes model in Eq. (2). (2) We fitted the imaginary part of the pseudodielectric function $\langle \epsilon_2 \rangle$ and the pseudo-loss function $\langle \eta_2 \rangle$, see Eq. (S6), with a Lorentzian to obtain the TO and LO broadenings, respectively. Both methods yield the same broadenings for the LO phonon, but not for the TO phonon. We therefore discuss how the choice of the TO broadenings in the models affects the agreement with the experimental data. Since the Raman line-shapes of the TO and LO phonons closely follow the peaks of ϵ_2 and the loss function,⁷ it is not surprising that the second method provides better agreement with the Raman broadenings determined by Bairamov *et al.*²⁰

To investigate this question, we show the ellipsometric angles ψ and Δ , the imaginary part $\langle \epsilon_2 \rangle$ of the pseudo-dielectric function, and the pseudo-loss function $-\langle \eta_2 \rangle$ versus photon energy for GaP at three different temperatures in Figs. S3, S4, and S5 (symbols). The Lowndes model (shown by red lines), fitted to the ellipsometric angles, describes the ellipsometric angles and the pseudo-loss function very well, but it significantly overshoots the magnitude of the peak in $\langle \epsilon_2 \rangle$. Since the resolution of the ellipsometer was set to 1 cm^{-1} and the peak width at room temperature is $\gamma_{\text{TO}}=2.9 \text{ cm}^{-1}$, we do not believe that this is an issue with the instrumental resolution. The asymmetry of the $\langle \epsilon_2 \rangle$ peak also does not explain this discrepancy. Perhaps small systematic errors in the ellipsometric angles lead to large errors in $\langle \epsilon_2 \rangle$, especially for very large values of $\langle \epsilon_2 \rangle$.

Fitting the ellipsometric angles with a Lorentzian (shown in blue in Figs. S3, S4, and S5) overshoots the $\langle \epsilon_2 \rangle$ peak even more. In this case, the fit arrives at a low value of γ , because the same broadening is used for the TO and LO phonons. The LO phonon broadening is very small and therefore the Lorentz fit takes an average value of the TO and LO broadenings as the Lorentzian broadening γ , which is too small. Therefore, we

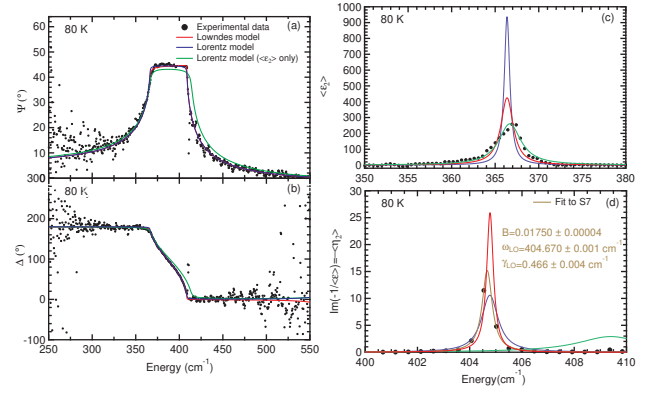


FIG. S3. Ellipsometric angles (a) ψ and (b) Δ , (c) imaginary part $\langle \epsilon_2 \rangle$ of the pseudo-dielectric function, and (d) pseudo-loss function $-\langle \eta_2 \rangle$ versus photon energy for GaP at 80 K (symbols) fitted with two different Lorentz models (blue, green) with different broadening parameters. A Lowndes fit (red) is also shown. The pseudo-loss function is also fitted with a Lorentzian, compare Eq. (S7), shown by the brown line.

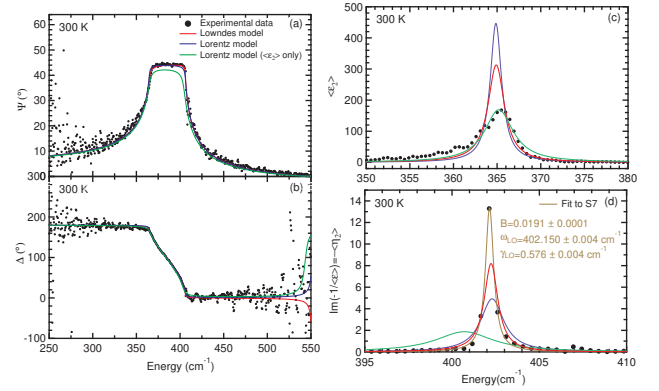


FIG. S4. Same as Fig. S3, but at 300 K (inside the cryostat). The parameters are slightly different from Fig. S1.

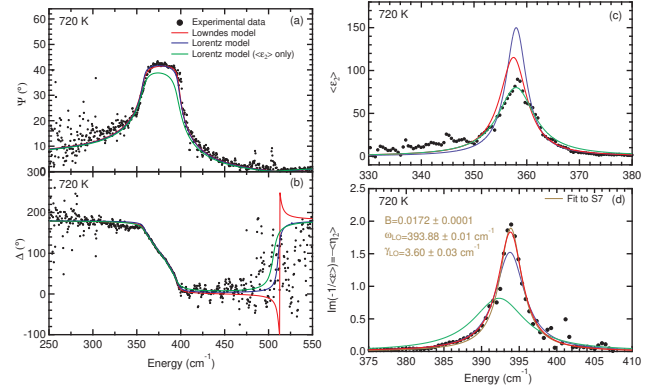


FIG. S5. Same as Fig. S3, but at 720 K.

understand why the Lorentzian fit to the ellipsometric angles overshoots the $\langle \varepsilon_2 \rangle$ peak.

Finally, we determine γ_{TO} by fitting the $\langle \varepsilon_2 \rangle$ peak with a Lorentzian (green line). We obtain a good fit to the data and the amplitude of the $\langle \varepsilon_2 \rangle$ peak is reproduced well. However, the large broadening leads to a poor fit of the ellipsometric angles and the pseudo-loss function peak. The peak value of the ψ -reststrahlen band is much lower in the model than in the data. Also, the falling slope near the LO energy is pushed too far towards larger energies. For completeness, we also show a Lorentzian fit to the pseudo-loss function peak (brown).

We noted earlier that the peak of the ψ -reststrahlen band strongly depends on the broadening. For $\gamma=0$, the maximum of ψ equals 45° and decreases with increasing γ between the TO and LO energies. Therefore, accurate measurements of ψ using spectroscopic ellipsometry allow accurate measurements of γ , even when the instrumental resolution is larger than γ . While absolute reflectance measurements are very difficult experimentally, the accuracy of ψ is usually better than 0.3° in the mid-infrared spectral range around $30 \mu\text{m}$ wavelength.

It is well known that the magnitude of the reststrahlen bands in GaP reflection measurements is influenced by polishing and etching, presumably due to changes in surface roughness.⁴⁵ A poorly prepared surface will reduce the measured reflectance or the ellipsometric angle ψ . Since our value of ψ is above 44° at room temperature, our surface quality is excellent and does not explain the broad $\langle \varepsilon_2 \rangle$ peak.

S4. RELATIONSHIP BETWEEN PHONON LIFETIMES AND BROADENINGS

According to Laubereau and Kaiser⁴⁰ and Kuhl and Bron,³⁶ the relationship between the broadening of the Raman phonon in wave numbers $\Delta\bar{\nu}$ and the phonon dephasing time (coherence time, or simply lifetime) $\tau=T_2$ is

$$\Delta\bar{\nu} = \frac{1}{\pi c \tau}, \quad (\text{S11})$$

where c is the speed of light. The phonon wave number $\bar{\nu}$ is related to its wavelength λ and its energy E through

$$hc\bar{\nu} = \frac{hc}{\lambda} = hf = E, \quad (\text{S12})$$

where h is Plack's constant. Therefore,

$$\gamma = \Delta E = hc\Delta\bar{\nu} = \frac{hc}{\pi c \tau} = \frac{h/2\pi}{\pi \tau/2\pi} = \frac{\hbar}{\tau/2} = \frac{2\hbar}{\tau}. \quad (\text{S13})$$

Kuhl and Bron³⁶ found a dephasing time T_2 for GaP at room temperature of 14 ps. The coherent anti-Stokes Raman decay constant $T_2/2$ is therefore 7 ps. The corresponding Raman broadening γ equals 0.094 meV or 0.76 cm^{-1} , as shown in Fig. 2 of Kuhl and Bron.³⁶

A different perspective is given by von der Linde, Kuhl, and Klingenberg.⁴¹ For GaAs at 77 K, they list a phonon lifetime of $\tau=6.3$ ps and a broadening $\Delta\bar{\nu}=0.85 \text{ cm}^{-1}$ or $\gamma=0.10$ meV.

This suggests a relationship similar to the radiative broadening of Loudon³⁹

$$\gamma = \frac{\hbar}{\tau}. \quad (\text{S14})$$

Laubereau, von der Linde, and Kaiser⁴² also employ Eq. (S14). Equations (S13) and (S14) differ by a factor of two.

In some publications^{26,39} (R. F. Wallis, I. P. Ipatova, and A. A. Maradudin, *Fiz. Tverd. Tela* **8**, 1064, 1966; *Sov. Phys. Solid State* **8**, 850, 1966), the full width at half maximum (FWHM) of a Lorentzian is taken to be $\gamma=2\gamma'$. In that case

$$2\gamma' = \frac{\hbar}{\tau} \quad \text{or} \quad \gamma' = \frac{\hbar}{2\tau}. \quad (\text{S15})$$

This convention is related to the identity

$$\begin{aligned} \varepsilon(\omega) &= \varepsilon_\infty + A \left(\frac{1}{\omega_0 - \omega - i\gamma'} + \frac{1}{\omega_0 + \omega + i\gamma'} \right) = \\ &= \varepsilon_\infty + \frac{2A\omega_0}{(\omega_0^2 + \gamma'^2) - \omega^2 - 2i\gamma'\omega}. \end{aligned} \quad (\text{S16})$$

In other words, Eq. (S16) indicates that the sum of two complex-conjugate harmonic terms with broadening γ' equals a Lorentzian with a full width at half maximum (FWHM) of $2\gamma'$. Note also the shift of the resonance frequency due to broadening. Compare Loudon³⁹ and the WVASE32 software guide published by the J. A. Woollam Co.

For our work described in this manuscript, we follow Eq. (S13) from Laubereau and Kaiser.⁴⁰

S5. ORIGIN OF THE TO AND LO PHONON BROADENINGS

In the main manuscript we interpreted the TO and LO broadenings as pure lifetime broadenings, but we should also discuss other potential contributions to the phonon broadenings. To this end, we first calculate the optical penetration depth d_{opt} (the inverse of the absorption coefficient α) from our model, see Fig. S6.

We find that the penetration depth is 200 nm at the TO energy and even larger at different photon energies. Therefore, the width of our phonon peaks is not likely influenced by polishing damage near the surface. Of course, we are not able to rule out other inhomogeneous broadening mechanics, such as crystal defects or impurities.

The finite penetration depth also leads to an uncertainty

$$\Delta q = \frac{2\pi}{d_{\text{opt}}} \sim 0.005 \frac{2\pi}{a} \quad (\text{S17})$$

of the phonon wave vector, where a is the lattice constant of GaP. We find the corresponding uncertainty ΔE by calculating the phonon dispersion of GaP from a ten-parameter shell model¹⁵ using the programs of Kunc and Nielsen (*Comput. Phys. Commun.* **17**, 413, 1979) as shown in Fig. S7. For our (111) oriented sample, the uncertainty is along the Λ -direction. We find that the finite penetration depth causes

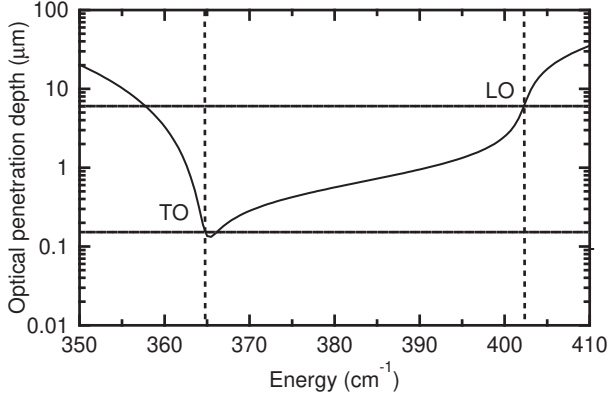


FIG. S6. Optical penetration depth for GaP in the reststrahlen region as a function of photon energy.

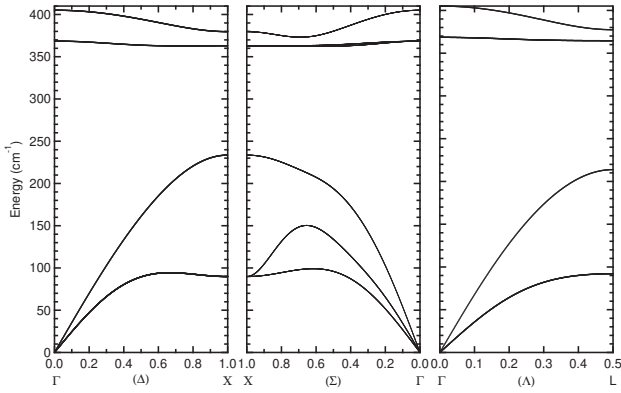


FIG. S7. Phonon dispersion curves for GaP, calculated using a ten-parameter shell model.¹⁵

an energy broadening of no more than 0.002 cm^{-1} , much smaller than our spectrometer resolution (1 cm^{-1}). Therefore, we conclude that the finite penetration depth does not have a significant impact on the phonon broadenings of GaP. By contrast, the finite penetration depth of x-rays determines the widths of Bragg reflections in C, Si, and Ge (Pietsch, Holy, Baumbach, *High-Resolution X-Ray Scattering*, Springer, New York, 2004, Fig. 1.5).

Finally, we discuss the impact of doping on the optical phonon broadenings. For an effective electron Drude (or conductivity) mass of (P. Kühne, T. Hofmann, C. M. Herzinger, and M. Schubert, *Thin Solid Films* **519**, 2613, 2011)

$$m_{cc} = \frac{3m_l m_t}{2m_l + m_t} = 0.35m_0 \quad (\text{S18})$$

for GaP in the X-valley (where $m_l=1.12m_0$ and $m_t=0.22m_0$ are the longitudinal and transverse masses, respectively, and m_0 is the free electron mass) and an electron concentration near $5 \times 10^{16} \text{ cm}^{-3}$, the screened plasma frequency⁸ ω_p is about 5 meV or 40 cm^{-1} . The lower (LP) and upper phonon-plasmon (UP) resonances are therefore given by (Varga, *Phys. Rev.* **137**, A1896, 1965; Mooradian and Wright, *Phys. Rev. Lett.*

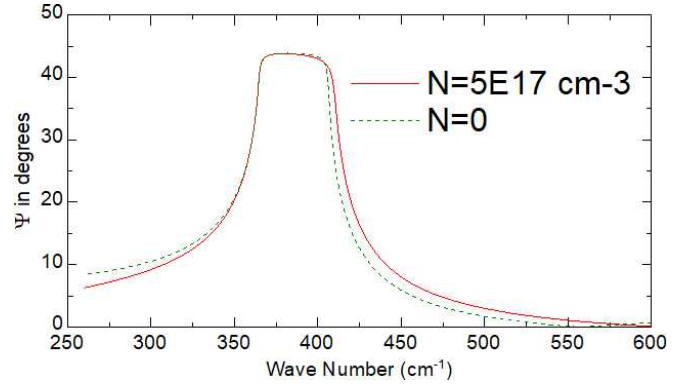


FIG. S8. Doping dependence of the ellipsometric angle ψ for bulk GaP at room temperature and 70° angle of incidence.

16, 999, 1966; Kukharskii, *Solid State Commun.* **13**, 1761, 1973)

$$\omega_{LP,UP}^2 = \frac{1}{2} (\omega_p^2 + \omega_{LO}^2) \pm \sqrt{\frac{1}{4} (\omega_p^2 + \omega_{LO}^2)^2 - \omega_p^2 \omega_{TO}^2}. \quad (\text{S19})$$

The UP energy is the experimentally measured LO energy modified by doping.

Using $\omega_p=40 \text{ cm}^{-1}$, $\omega_{TO}=364.8 \text{ cm}^{-1}$, and $\omega_{LO}=401.9 \text{ cm}^{-1}$, we find $\omega_{LP}=36.3 \text{ cm}^{-1}$ (below our spectral range) and $\omega_{UP}=402.3 \text{ cm}^{-1}$. This means that the “true” LO energy for an undoped sample is about 0.4 cm^{-1} below our measured value of 402.3 cm^{-1} for our electron concentration of $5 \times 10^{16} \text{ cm}^{-3}$. This might explain small variations of the reported values of ω_{LO} in the literature, if no doping correction was performed.

With increasing doping concentration, the UP broadening (i.e., the observed LO broadening due to the interaction between the LO phonon and free carriers) increases considerably, while the TO phonon broadening remains about the same (Kukharskii 1973). This was observed in two different studies by Bairamov *et al.*,^{20,21} where the sample with the higher resistivity of 10^{10} - $10^{12} \Omega\text{cm}$ had an LO broadening of 0.6 cm^{-1} , while a less pure sample with a carrier concentration of $9 \times 10^{16} \text{ cm}^{-3}$ had an LO broadening of 2 cm^{-1} , see Table I. Therefore, free-carrier effects cannot explain why the TO broadening is larger than the LO broadening. We also verified this by adding the effects of free carriers in our ellipsometry model with a Drude term. As shown in Fig. S8, the ellipsometric angle ψ for a 70° angle of incidence depends on the doping level for carrier concentrations exceeding $5 \times 10^{17} \text{ cm}^{-3}$, one order of magnitude higher than for our sample. For this simulation we assumed a mobility of $375 \text{ cm}^2/\text{Vs}$ (independent of carrier concentration), calculated from the resistivity of $0.3 \Omega\text{cm}$ specified by the supplier of this sample.

Since we perform measurements at elevated temperatures, one might also ask if the density of thermally excited carriers can contribute to the broadenings of LO phonons. We therefore calculated the intrinsic carrier density (N. W. Ashcroft and N. D. Mermin, *Solid State Physics*, Saunders, Fort Worth,

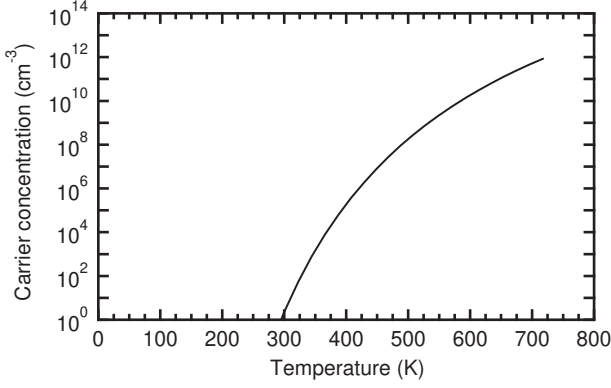


FIG. S9. Intrinsic carrier concentration of GaP as a function of temperature calculated from Eq. (S20).

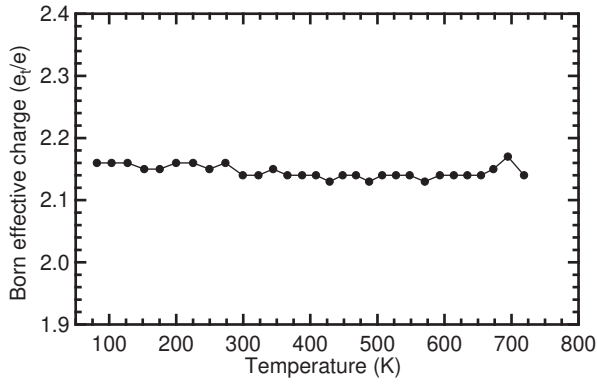


FIG. S10. Temperature dependence of the Born effective charge calculated from Eq. (S22) for bulk GaP.

1976, p. 575)

$$n_i(T) = \frac{1}{4} \left(\frac{2k_B T}{\pi \hbar^2} \right)^{3/2} (m_c m_v)^{3/4} e^{-\frac{E_g}{2k_B T}} = \quad (S20)$$

$$= 2.5 \left(\frac{m_c m_v}{m_0^2} \right)^{3/4} \left(\frac{T}{300 \text{ K}} \right)^{3/2} e^{-\frac{E_g}{2k_B T}} \times 10^{19} \text{ cm}^{-3}.$$

Here we need to use the density of states mass for electrons

$$m_c = N_v^{2/3} \sqrt[3]{m_l m_l^2} = 0.79 m_0, \quad (S21)$$

where $N_v=3$ is the number of X -valleys. The other parameters are $m_v=0.83m_0$ and $E_g=2.25$ eV. The results of calculating the intrinsic carrier density (S20) are shown in Fig. S9. Even at our highest temperatures, the intrinsic density of thermally excited carriers is many orders of magnitude lower than the doping concentration of $5 \times 10^{16} \text{ cm}^{-3}$ and therefore can be ignored.

S6. GAP BORN EFFECTIVE CHARGE

In a polar crystal, there is a charge transfer between the atoms involved in the chemical bond. This is known as the

Born effective charge e_i^* . It does not have a large influence on the energies of long-wavelength TO phonons, but it adds an additional Coulombic restoring force to the long-wavelength LO vibrations (Fröhlich interaction). This leads to a splitting of the TO and LO phonons at the Γ -point. From this Fröhlich splitting, the Born effective charge

$$e_i^* = \sqrt{V \mu \epsilon_0 \epsilon_\infty (\omega_{LO}^2 - \omega_{TO}^2)} \quad (S22)$$

can be calculated at each temperature, see Reparaz *et al.*, Appl. Phys. Lett. **96**, 231906 (2010). V is the volume per GaP formula unit (volume of the primitive unit cell), μ the reduced mass of the Ga and P atoms, ϵ_0 the vacuum permittivity, and ϵ_∞ the high-frequency dielectric constant. As shown in Fig. S10, the Born effective charge does not depend on temperature, as one would expect. The average Born effective charge is 2.15(1) over the whole temperature range. We did not observe the small increase in the Born effective charge with temperature due to thermal expansion predicted by Debernardi.¹⁰

S7. VARIATION OF THE APPARENT GAP SURFACE LAYER THICKNESS

Insulators are mostly transparent in the mid-infrared spectral region, above the phonon absorption energies and below the band gap. In this region, the ellipsometric angle Δ must be 0 or π for a bare substrate, depending on the relative magnitude of the angle of incidence and the Brewster angle. Experimentally, one observes deviations of Δ from the ideal values for two reasons: (1) Surface overlayers, such as surface roughness, native oxides, or adsorbed overlayers such as water, ice, or other airborne molecular contamination. See G. E. Jellison and B. C. Sales, Appl. Opt. **30**, 4310 (1991). (2) Systematic errors affecting the measurement of Δ , especially those caused by the diamond windows of our UHV cryostat.³⁰

In Fig. S11, we report the surface layer thickness in our experiments, modeled as a 50/50 mixture of GaP and voids within the Bruggeman effective medium approximation. We

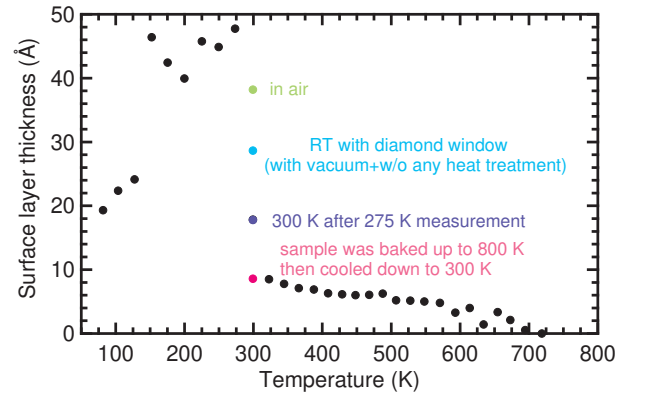


FIG. S11. Variation of the apparent GaP surface layer thickness with temperature.

call this the *apparent* surface layer thickness, because it might be affected by systematic errors from the cryostat windows.

An initial measurement of the GaP sample in air (without windows) finds a surface layer thickness of 38 Å, shown by the green data point. The sample is then mounted in the cryostat followed by pumping to UHV conditions. This reduces the surface layer thickness to 29 Å, as shown by the blue data point. This reduction might be due evaporation of some of the overlayer, but it could also be due to errors caused by our windows. We then heat the sample to 800 K for several hours and let it cool down to room temperature overnight. This reduces the surface layer thickness to 9 Å, as shown by the red data point. Most likely, this value of 9 Å represents the residual surface roughness, after all adsorbed contaminants have evaporated.

We now start our temperature series at 80 K, where the surface layer thickness is 19 Å. We gradually increase the temperature to 275 K and measure the pseudo-dielectric function at each step for several hours. This increases the surface layer thickness to 48 Å, as ice forms on the sample. At the next temperature (300 K), the surface layer thickness is only 18 Å, because most of the ice has evaporated. As we heat the sample to 325 K, the surface layer thickness is 8 Å and it gradually is reduced to zero as we heat towards 700 K. It is not likely that the surface layer thickness will actually vanish at 700 K. It is more likely that our data are affected by experimental errors due to the diamond windows. These windows are not getting warm, even at the highest sample temperatures. Therefore, the errors due to the windows are likely independent of temperature. It is likely that we underestimate the surface layer thickness in the cryostat by about 10 Å, due to the retardance of the diamond windows.

This discussion emphasizes that one must be careful when interpreting changes of optical constants with temperature. A careful preparation of the sample is required to minimize surface overlayers. It can be very helpful to heat the sample for several hours to reduce airborne molecular contamination, if this does not change the properties of the sample. It is inevitable for ice to form on the sample below room temperature, even under the best (10^{-8} Torr) vacuum conditions achievable in our setup.